

HF Induced Modifications of the Electron Density Profile in the Earth's Ionosphere Using the Pump Frequencies Near the Fourth Electron Gyroharmonic

A. V. Shindin^{1*}, E. N. Sergeev¹, S. M. Grach¹, G. M. Milikh^{2†}, P. A. Bernhardt^{3‡}, C. Siefring³, and M. J. McCarrik⁴

¹Lobachevsky University of Nizhny Novgorod

²University of Maryland

³Plasma Physics Division, Naval Research Laboratory

⁴Information Technology Division, Naval Research Laboratory

Key Points:

- plasma profile modifications in the HF-pumped ionosphere with frequencies near the fourth electron gyroharmonic are studied at HAARP
- plasma expulsion from the reflection height and the upper hybrid height of the pump wave were detected
- The expulsion from the upper hybrid height had been strongly suppressed for the pump frequency close to fourth electron gyroharmonic

*Gagarin av. 23, Nizhni Novgorod, 603950, Russia

†College Park, MD, 20742-2421, USA

‡Naval Research Laboratory, Washington, DC 20375, USA

Corresponding author: A. V. Shindin, shindin@rf.unn.ru

Abstract

We discuss results on plasma density profile modifications in the F-region ionosphere caused by HF heating with the frequency f_0 in the range $[(-150 \text{ kHz})-(+75 \text{ kHz})]$ around the 4th electron gyroharmonic $4f_c$. The experiments were conducted at the HAARP facility on June 2014. The multi-frequency Doppler Sounder (MDS) which measures the phase and amplitude of reflected sounding radio waves complemented by the observations of the Stimulated Electromagnetic Emission (SEE) were used for the diagnostics of the plasma perturbations. We detected noticeable plasma expulsion from the reflection region of the pumping wave, and from the upper hybrid region, the expulsion from the latter one had been strongly suppressed for $f_0 \approx 4f_c$. The plasma expulsion from the upper hybrid region was accompanied with the sounding wave's anomalous absorption slower developing for $f_0 \approx 4f_c$. Also, slower developing and weaker expulsion was detected for the height region between the pump wave reflection and upper hybrid altitudes.

Plain Language Summary

We report first results of systematic studying electron density profile modifications in the F-region of the ionosphere caused by HF heating with the pumping frequencies in the range $[(-150 \text{ kHz})-(+75 \text{ kHz})]$ near the 4th electron gyroharmonic at the HAARP heating facility. We measured phase and amplitude of ionospherically reflected sounding waves simultaneously with Stimulated Electromagnetic Emission. The phase data allowed determining electron density profile evolution, the amplitude data provide information of the pump-induced sounding waves' absorption, while SEE allows estimating offset between the pump frequency and gyroharmonic. We detected noticeable plasma expulsion from the reflection height and slower developing expulsion from the upper hybrid height of the pump wave. Even slower developing and weaker expulsion was detected for the height region between the pump wave reflection and upper hybrid heights. The plasma expulsion from the upper hybrid region was accompanied with the sounding wave's anomalous absorption, but was strongly suppressed for the pump wave frequency close to fourth electron gyroharmonic, when the prominent "Downshifted Maximum" in SEE was quenched. The combined phase sounding and SEE measurements allowed obtaining interconnection between different manifestations of the HF-induced turbulence and determining altitude of the most effective pump wave energy input to ionospheric plasma.

1 Introduction

A powerful O-mode electromagnetic pump wave transmitted from the ground into the bottom-site ionospheric F region excites a wide range of plasma processes leading to the appearance of artificial ionospheric turbulence (AIT), i.e., generation of different HF and LF plasma modes, plasma density inhomogeneities of scales from tens of centimeters to kilometers, causes electron heating, electron acceleration, ionization, generation of ionospheric airglow etc. (Gurevich, 2007; Grach et al., 2016; Streltsov et al., 2018). Diverse diagnostic methods and tools are used for the AIT studying, particularly, sounding of the heated volume of the ionosphere by diagnostic waves and a registration of secondary, or stimulated, emission (SEE) in different frequency ranges.

The pump-plasma interaction is known to be strongest near the pump reflection height z_{r_0} at which $fp(z_{r_0})$ equals the pump frequency f_0 , and near the upper hybrid (UH) resonance height z_{UH} where $f_p(z_{UH}) = (f_0^2 - f_c^2)^{1/2}$ [here $fp = (e^2 N / \pi m)^{1/2}$, and $f_c = eB / (2\pi mc)$ are the electron plasma frequency and the electron cyclotron frequency, e and m are the electron charge and mass, N the electron density, c the speed of light, B the geomagnetic field strength]. This corresponds to existing theoretical concepts and is confirmed by investigations of the HF-pumped ionospheric volume by multifrequency Doppler sounding (MDS) at SURA and EISCAT heating facilities (Vaskov

et al., 1986; Berezin et al., 1991; Lobachevsky et al., 1992; Grach et al., 1997; A. Shindin et al., 2012), which have revealed plasma expulsion from the resonance regions.

Stimulated electromagnetic emission (SEE) with frequencies f_{SEE} close to the pump wave frequency f_0 occurs due to conversion of HF pump-driven electrostatic plasma modes, most notably Langmuir (L) and upper hybrid (UH), into electromagnetic waves smaller than the reflected pump wave (PW) by 50-90 dB (Thidé et al., 1982; Stubbe et al., 1984; Leyser et al., 1989) and provides rich information about AIT (Grach et al., 2016). SEE spectral characteristics depend on $\Delta f_c = f_0 - nf_c$, the offset of the pumping wave (PW) frequency f_0 from the multiple electron gyroresonance nf_c , the most dramatic changes occur during transition of f_0 via nf_c (e.g. from $f_0 < nf_c$ to $f_0 > nf_c$) and allows one to estimate Δf_c during the experiment (Leyser et al., 1993; Leyser, 2001; Frolov et al., 2001; Sergeev et al., 2006; Grach et al., 2008, 2016).

We report results of the first experiments using MDS (phase) sounding of the HF-pumped ionosphere at the HAARP heating facility, located near Gakona, Alaska, USA (62.40°N, 145.15°W) performed on June 2014. Simultaneously the SEE was monitored, and the anomalous absorption (AA) of sounding waves was measured. The heating facility was used both for the pump wave radiation and as pulsed Doppler HF radar. The main purpose of the experiments was to study the dependence of HF-pump-induced electron density expulsion from the resonance regions (in correlation with the AA and SEE) on the offset of the pump wave frequency from the fourth gyroharmonic, $\Delta f_c = f_0 - 4f_c$, the experiment was performed for.

2 Experimental Setup

Experiments on phase-amplitude sounding of the ionosphere heated volume were performed on June 4. During time interval 14:55-16:25 AKDT the HAARP transmitter radiation schedule was organized as a sequence cycles at different PW frequencies f_0 varied from 5540 till 5730 kHz. The choice of the PW frequency nominals was conditioned by covering available range around $4f_c$. Each cycle was organized as follows. During 4.5 min the HAARP operated as pulsed Doppler HF radar. The transmitters radiated vertically low-duty cycle diagnostic waves (DW): short (20 μ s) pulses with the interpulse period $T = 100$ ms at two carrier frequencies $f_{\text{DW}} = f_0$ and $f_{\text{DW}} = f_0 - 200$ kHz with effective radiated power (ERP) $P_{\text{ef}} \sim 400$ MW each. After 30 seconds the radar mode was combined for 45 seconds with quasi-continuous wave (QCW) pumping mode, i.e. high duty cycle pump wave (pulse width $\tau = 70$ ms, the same interpulse period $T = 100$ ms) at a frequency f_0 with the same ERP. During the QCW, the short pulses were radiated at 20th ms of the 30 ms pauses. After switching off the radar mode, the 30 s pause of the HAARP transmitters was used for taking ionograms and changing the PW and DW frequencies. Then the 5-min cycle was repeated at the new f_0 and f_{DW} . The power of the 20 μ s diagnostic pulses was sufficient to create a wide spectrum of DW (up to 300 kHz near each carrier frequency). An average DW power $\langle P \rangle = P/Q = 80$ kW was far below the thresholds of the generation and maintenance of the pump-induced thermal plasma instabilities in the ionosphere (Grach et al., 1981). Also, the diagnostic pulses were too short to excite ponderomotive instability in the ionosphere (Frolov et al., 2007; Sergeev et al., 2007).

Under the combined radiation mode, the QCW created a perturbation in the ionosphere, particularly at the plasma resonance (reflection altitude of the pump wave) and at the UH resonance, while the DW simultaneously provided diagnostics of AIT (Vaskov et al., 1986; Berezin et al., 1991; Grach et al., 1997; Sergeev et al., 2007, 2016; A. Shindin et al., 2012). The high power of the HAARP transmitters used for MDS, applying broadband radio receiver and specially developed signal processing algorithms have allowed studying evolution of amplitude (A_i) and phase (φ_i) of the various spectral components of the reflected DW (with frequencies f_i), which passed the perturbed region twice, in

a wide frequency range $\Delta f_{\text{total}} \sim 600\text{kHz}$, ($-450\text{ kHz} \lesssim f_i - f_0 \lesssim +150\text{ kHz}$), and therefore, in a wide (till 25-35 km) altitude interval. Sometimes during QCW we could analyze spectral components of the radar pulses in smaller range $\Delta f_{\text{QCW}} \sim 360\text{ kHz}$ ($-280\text{ kHz} \lesssim f_i - f_0 \lesssim +80\text{ kHz}$). Outside of this range reflected signal fell till the background noise due to the anomalous absorption (AA, see below), and signal amplitude and phase analysis gave condemned results. The frequency resolution used for the analysis was 1 kHz; the temporal resolution was determined by the interpulse period $T = 100\text{ ms}$. The observational site were located, nearly under the heated region during injections at vertical. A 30-m folded-dipole BWDS receiver antenna was used in measurements. The receiver digitized a band 850 kHz, the dynamic range of the instruments after spectral processing is estimated to be better than 90 dB.

Figures 1 and 2 present results obtained during the cycles at $f_0 = 5540, 5600, 5660$ and 5730 kHz . Figure 1 shows the temporal evolution of Doppler frequency shifts $f_{di}(f_i, t) = d\varphi_i/dt$ (column a, φ_i is the phase incursion), normalized intensities $G_i(f_i, t)$ of the reflected DW spectral components (column b), and SEE spectrograms (column c). The DW intensities $A_i^2(f_i, t)$ are normalized to the $\langle A_i^2 \rangle$, the intensity averaged over 30 s before the QCW switching on, $G_i[\text{dB}] = 10 \log(A_i^2/\langle A_i^2 \rangle)$ characterizes the anomalous absorption (AA) due to scattering of DW into plasma (UH) waves on small-scale plasma density irregularities (striations). In Fig. 2b we used running averaging over 5 pulses (0.5 s). In the spectrograms, prominent spectral SEE features are marked. There are the L-related ponderomotive narrow continuum (NCp) and UH-related downshifted maximum (DM), 2DM, upshifted maximum (UM), thermal narrow continuum (NCt), broad continuum (BC) and broad upshifted maximum (BUM). Stationary peculiarities and temporal evolution of different SEE features are well described in numerous papers, see, e.g., (Frolov, 2004; Leyser et al., 1993, 1994; Leyser, 2001; Carozzi, 2002; Thidé et al., 2005; Sergeev et al., 2006; Kotov et al., 2008; Grach et al., 2008, 2016), etc. The SEE can be used for rough estimations of the offsets between f_0 and $4f_c$, $\Delta f_c = f_0 - 4f_c$, in the range between successive gyroharmonics. Most precisely this can be done for $f_0 \approx 4f_c$ and $f_0 \gtrsim 4f_c$ (see formulas (7) and (8) below).

3 Phase Data Processing

For all f_0 , when heating (QCW) is turned on, as a rule, an increase of all f_i (positive Doppler frequency shifts f_{di}) is often observed. It is less pronounced for narrow ranges of the diagnostic (sounding) waves frequencies with reflection heights near PW reflection and UH heights z_{r0} and z_{UH} , i.e. for $f_i \sim f_p(z_{r0})$ and $f_i \sim f_p(z_{UH})$. Negative f_{di} are observed after the heating turns off. Such pump-induced changes of f_{di} occur on the background of natural variations of the reflection heights (and f_{di}), determined by the motion of the ionosphere. The measured temporal evolution of Doppler frequency shifts $f_{di}(t) = d\varphi_i/dt$ for different f_i (Figure 1, panels a) provided data for the reconstruction of the electron density profile temporal evolution $N(z, t)$ in the HF-pumped ionosphere by solving the inverse problem of the phase sounding.

Under geometric optics approximation, each of the sounding waves at the angular frequency $\omega_i = 2\pi f_i$ propagating from the ground up to the reflection points $z_r(f_i)$ and back to the ground, experiences the phase incursion (Ginzburg, 1970):

$$\varphi(\omega, t) = \frac{2\omega}{c} \int_0^{z_r} n(\omega, \omega_p(z, t)) dz - \frac{\pi}{2} \quad (1)$$

where $\omega_p(z, t) = 2\pi f_p(z, t)$ is the plasma frequency, $n(\omega, \omega_p(z, t))$ is the wave refractive index. The reflection altitude z_r is determined by the condition $n = 0$, and t is the time. This can be translated in the following expression for an additional phase change $\Delta\varphi(\omega) = \varphi(\omega, t_0) - \varphi(\omega, t)$ in the time interval $[t_0, t]$ associated with perturbation of the

profile $N(z, t)$ due to ionosphere HF-pumping or to natural reasons:

$$y(\omega) = \frac{c}{2\omega} \Delta\varphi(\omega) = \int_{\omega_{\min}}^{g(\omega)} K(\omega, \omega_p) \Delta z(\omega_p) d\omega_p \quad (2)$$

Here $K(\omega, \omega_p) = dn(\omega, \omega_p)/d\omega_p$ is a kernel of the integral equation (2), $g(\omega)$ is the angular plasma frequency at the reflection point, which is $g(\omega) = \omega$ for an ordinary wave, t_0 is initial time, $\Delta z(\omega_p, t) = z(\omega_p, t) - z(\omega_p, t_0)$ is the altitude shift, i.e., the difference between the sounding radio wave reflection altitude at the current (t) and initial (t_0) times. Here the variable of the integration is replaced from the altitude z in (1) to the plasma frequency ω_p in (2). It is taken into account that at the reflection point $n(\omega, g(\omega)) = 0$, and at the entrance to the plasma layer $\Delta z = 0$. The left hand side $y(\omega)$ in (2) is to be determined from the experimental data as $\Delta\varphi_i = \int_{t_0}^t f_{di}(t') dt'$. On the base of the data obtained, an array $\Delta\Phi(\omega, t) = \Delta\varphi(\omega, t) - \Delta\varphi(\omega_{\min}, t)$ was created for the phase shifts $\Delta\varphi(\omega, t)$ of the diagnostic waves. Here ω_{\min} is least of the probe wave frequencies, in our experiment we have taken $\omega_{\min} = \omega_0 - 2\pi \cdot 280$ kHz. The probe wave at this frequency was reflected noticeably below ($\sim 25 - 35$ km) z_{UH} , and we assumed that the phase evolutions for this and lower frequencies do not depend on the pump-induced processes in the plasma resonance regions. This is confirmed, in particular, by measurements of the AA bandwidth of the DW (Fig. 1b). Also, the subtraction of $\Delta\varphi(\omega_{\min}, t)$ allows to exclude processes responsible for plasma density variations at lower altitudes caused by violation of the balance between ionization and recombination in the lower ionosphere.

For the exact expression of the refractive index for magnetized plasma, the equation (2) cannot be reduced to the analytically solvable integral equation. In this case, we had applied in (A. Shindin et al., 2012; Sergeev et al., 2016) the regularization algorithms by Tikhonov (1995) and solved the inverse problem numerically. In this paper, instead of numerical Tikhonov algorithm, we used an approximate expression for well describing ordinary wave refractive index near the reflection point for HAARP experimental conditions,

$$n(\omega, \omega_p) \approx \left(1 - \frac{\omega_p^2}{\omega^2}\right)^\beta, \quad \beta \approx 0.29. \quad (3)$$

Substituting (3) into (2), we obtain the generalized Abel equation (Korn & Korn, 2000):

$$\int_{\omega_{\min}^2}^{\omega^2} \frac{\Delta z}{(\omega^2 - \omega_p^2)^{1-\beta}} d\omega_p^2 = F(\omega), \quad F(\omega) = -c \frac{\omega^{2\beta-1}}{2\beta} \Delta\varphi(\omega) \quad (4)$$

with the solution

$$\Delta z = \frac{\sin\{\pi(1-\beta)\}}{\pi(1-\beta)} \int_{\omega_{\min}^2}^{\omega^2} \frac{F'(\omega_p^2)}{(\omega^2 - \omega_p^2)^\beta} d\omega_p^2. \quad (5)$$

Dynamics of the reflection altitude shifts of different DW spectral components, $\Delta z_r(\omega_i = 2\pi f_i, t)$ is displayed in Figure 2, panels a. In this figure $t = 0$ corresponds to QCW switching on, blue and red lines correspond to the reflection altitude of the DW at $f_i = f_0$, i.e. the PW reflection altitude, ($z(f_i) = z_r(f_0)$) and to the reflection altitude of the DW at $f_i = f_p(z_{UH}) = (f_0^2 - f_c^2)^{1/2}$, i.e. reflection from the pump wave UH resonance height, respectively. Chosen frequency step between neighbor spectral components displayed in the Figure 2a is $\Delta f = 30$ kHz. For clarity we introduce additional height shift 300 m between reflection altitude shifts of the successive DW spectral components at $t = 0$.

Temporal variations of the reflection heights $\Delta z(f_i, t)$ allows to calculate velocities of the vertical motion of plasma density at a certain magnitude $Ni = \pi f_i^2 m / e^2$ as $V_v = \partial \Delta z_r(f_i, t) / \partial t$ at different f_i . The velocities of the sounding waves reflection height displacement vs. time and sounding wave frequency (pulse spectral component) $V_v(f_i, t)$ are presented in Figure 2b. Positive (red) velocity values correspond to upward motion of a certain plasma density level while negative (blue) values correspond to downward motion.

Calculating the altitude shifts $\Delta z_r(f_i, t)$ allows us observing the evolution of the electron density profile $N(z, t)$ from the reference one. The reference profile $N_0 = N(z, t_0)$ is taken from ionogram registered prior to the QCW pumping session. For this we shall transform $\Delta z_r(f_i, t)$ to $\Delta z_r(N, t)$ by using the univocal relation between the plasma frequency at the radio wave reflection point and electron density. Therefore,

$$z(N, N_0, t) = z(N_0) + \Delta z(N, t) \quad (6)$$

is the dependence of the reflection height of the radio wave on the density. Then we find the required distribution $N(z, t)$ by calculating the inverse of (6). Relative differences between reconstructed and reference electron density profiles $\delta N(z, t) = [N(z, t) - N_0]/N(z, t_0)$ vs. altitude z for all f_0 at 5th, 15th, 30th and 45th seconds of pumping are presented in Figure 2c.

Figure 2 illustrates the evolution of the electron density in the HF-pumped ionosphere in the altitude range from region above the reflection height till the region below the UH height.

4 Analysis of the Combined Phase sounding, AA, and SEE Data

Let's start an analysis from $f_0 = 5540$ kHz, the upper row of figures 1 and 2. During this cycle the pump frequency $f_0 = 5540$ kHz belongs to the “weak emission range” between 3rd and 4th gyroharmonic, where SEE spectrum contains weak BC, DM and UM (Fig. 1c). The offset $\Delta f_c = f_0 - 4f_c$ here can be roughly estimated from ionograms and geomagnetic field IGRF model as $\Delta f_c \sim -(130 - 150)$ kHz.

From Figure 1a, it is seen that immediately after QCW is switched on the Doppler frequency shifts were mainly positive ($f_{di} > 0$) for all spectral components except of ones close to the pump frequency ($f_i \approx f_0$) where $f_{di} < 0$. Such a behavior of f_{di} is translated to increasing reflection altitudes of the sounding waves z_{ri} with the frequencies close to the pump wave frequency f_0 (Fig. 2a) with velocities V_v up to 100 m/sec, and, to the contrary, slighter decreasing z_r for both $f_i > f_0$ and $f_i < f_0$ with velocities V_v up to 60 m/s (Fig. 2b). This corresponds to electron density decrease in the vicinity of the pump wave reflection height $z_{r0} = z_r(f_0)$ and increase on other heights, i. e. to the plasma expulsion from the reflection point vicinity. The relative density depletion (hereafter reflection depletion, RD) reaches up to $\sim 0.1 - 0.2\%$ at 5th second of the QCW pumping (Fig. 2c). According to Fig. 2a, the uplifting $\Delta z_r(f_i \approx f_0)$ grows from 0.1 s till (3-5) s, reaching 100-300 m, and then slows down till $t = 10-15$ s. The SEE feature NCp appears immediately after QCW switching on, simultaneously with the start of the plasma expulsion from the vicinity of z_{r0} and then exhibits strong overshoot-effect: its spectral width and intensity noticeably drops during the raise of $z_r(f_0)$ and growth of the AA and UH-related SEE features (Fig. 1b, 1c). Such initial behavior of the $f_d(f_i, t)$, $\Delta z_r(f_i, t)$, $V_v(f_i, t)$, , NCp and AA is qualitatively similar for all f_0 and does not depend on the offset Δf_c .

Few seconds later, in $t = 1-3$ s, phenomena related to excitation of the UH waves and striations, resulting in the phenomena such as the AA, and the UH related SEE features (DM, UM, and BC), and the plasma expulsion from the UH height region ($z \sim z_{UH}$, the “UH depletion”, hereafter UHD) developed simultaneously. The expulsion corresponded to appearance of the expanding range with $f_{di} < 0$ in Fig. 1a. At 3-5 s the UHD became deeper than the RD, and then the UHD developed monotonously till QCW pumping switchies off. At $t = 15$ s the uplifting near the reflection point accelerated again and continued till the QCW stops, for s deepening of the UHD and RD is accompanied by plasma density decrease in the whole altitude range (Fig. 2c).

For the cycle at $f_0 = 5600$ kHz (Figs. 1, 2, second row) the results of AA measurements (temporal development and magnitude) and the phase sounding analysis ($f_d(f_i, t)$,

$\Delta z_r(f_i, t)$, $V_v(f_i, t)$ and $\delta N(z, t)$) were similar to ones for $f_0 = 5540$ kHz, but their SEE were fairly differed. According to the SEE spectrogram (Fig. 1c), the PW frequency belongs to “below harmonic” range. It shows strong DM and resolved 2DM. The offset can be roughly estimated as $\Delta f_c \sim -(60 - 70)$ kHz. According to the ionograms, z_{UH} in the cycles at 5540 and 5600 kHz were close, $z_{UH} \sim 225$ km.

Note, during these cycles the average anomalous absorption $\langle G \rangle$ in the range $170 < f_0 - f_i < 220$ kHz decreased by $\sim 10 - 15$ dB (Figs 1b) in comparison with the range $-30 < f_0 - f_i < 150$ kHz. The most probably it can be attributed to focusing of HF diagnostic radio waves reflected from the UH altitudes with density depletion (Vaskov et al., 1986).

In the cycle at $f_0 = 5660$ kHz (Figs. 1, 2, 3rd row) the behavior of the bulk of investigated parameters differed noticeably from cycles at $f_0 = 5540$ and 5600 kHz.

The RD developed similar to cycles with other f_0 during first 10 s of QCW pumping, but did not slow down after 10 s of QCW pumping. Negative f_{di} appeared near $f_i(z_{r0})$ than the range of $f_{di} < 0$ expanded for mainly to lower f_i . Dependence looked like shallow quasi-periodic structure with a period $\sim 3-4$ km, amplitude growing in time and decreasing downward from z_{r0} , and occupying a height interval exceeding spacing between z_r and z_{UH} . The UHD and z_{UH} uplifting did not resolving in this cycle, moreover, the weak descending of the UH height at surrounded frequencies were observed. Then the AA developed slower than in other cycles, while attained the same magnitudes till 45th s. The difference is due to the fact that during this cycle at $f_0 = 5660$ kHz the pump wave frequency was much closer to the double resonance where $f_{UH} \approx 4f_c$. This is seen from the SEE spectrogram (Fig. 1c). Here the DM is not resolved till $t \sim 10-15$ s which means that

$$f_{DM} = f_0 - \Delta f_{DM} \approx f_{UH} \approx 4f_c \quad (7)$$

at the UH height (the “resonance range”), f_{DM} is the DM peak frequency. Then the DM appeared which was probably attributed to amplification of the $\delta N(z, t)$, and changing of the UH height, and therefore, a violation of (7). This allows to estimate the offset $\Delta f_c = f_0 - 4f_c$ during the cycle as 7-15 kHz: initially $\Delta f_c \approx \Delta f_{DM}$ and then changed. Detailed analysis of the SEE peculiarities (DM, UM and BUM) near the double resonance can be found in (Leyser et al., 1994; Carozzi, 2002; Sergeev et al., 2006; Kotov et al., 2008; Grach et al., 2008). Note that the altitude of the double resonance obtained from (7) and IGRF model ~ 240 km exceeded z_{UH} obtained from the ionogram by 10 km. This value fits into the error in determining the heights when processing ionograms.

The cycle at $f_0 = 5730$ kHz (Figs. 1, 2, row 3) was the only cycle with $f_0 > 4f_c$, the offset $\Delta f_c = f_0 - 4f_c$ can be estimated from the SEE spectrogram as

$$\Delta f_c = f_0 - 4f_c \approx f_{BUM} - f_0 = \Delta f_{BUM}, \quad (8)$$

$\Delta f_c \sim +75$ kHz (Fig. 1c), f_{BUM} is the BUM peak frequency. From Fig. 3 it can be concluded the following. After QCW pumping switching on the plasma expulsion from the vicinity of the reflection point (RD) and the NCp development in SEE spectrum behaved similarly to all f_0 . Slowing down of the RD deepening after development of the UH-related effects is were not observed. Like for $f_0 < 4f_c$, for $f_0 > 4f_c$ the UH-related effects, namely AA; DM, 2DM, UM, SEE features; and UHD developed few seconds later than L-related processes near the reflection height. The characteristics of this processes during this cycle, however, differed from ones for $f_0 < 4f_c$.

First, the AA attained a saturation at $t \sim 10-15$ s, but for $f_0 > 4f_c$ at the saturation stage $\langle G \rangle \sim 25 - 30$ dB, while at $f_0 < 4f_c$ $\langle G \rangle \sim 18 - 20$ dB, and the frequency range with strong AA is wider at $f_0 > 4f_c$ than at $f_0 < 4f_c$ (Figs 1b). Due to the strong AA, in the range $5590 < f_i < 5650$ kHz the DW signal intensity fell below the background noise, and measurements of Doppler shifts/phase incursions and AA

were contaminated. This range is shown in Figures 1,2, row 4 by double arrows and dashed parts of lines and shall be excluded from the analysis for $t > 15$ s. Second, the strong NCt showed up in the SEE spectrogram at $\Delta f \sim 0 - (-7)$ kHz with a temporal behavior similar to DM, 2DM and UM; after $t \sim 1.5$ s the NCt covered NCp. The DM, 2DM and UM developed concurrently with AA, exhibited the overshoot effect with maxima at $t \sim 6 - 11$ s, and were more intensive then in other cycles. Such SEE behavior is typical for the “above harmonic range” close to the “strong emission” range (Sergeev et al., 2006). Third, the UHD started to develop ~ 2 km above the nominal upper hybrid resonance height and occupied quite wide (> 5 km) altitude interval. Later, in $t \sim 10 - 15$ s, the interval expanded (till ~ 8 km) and descended below the UH height. During the whole 45 s of the QCW pumping the UHD remained shallower than the RD (Fig. 2c).

After the termination of the QCW, the signs of Doppler frequency shifts f_{di} and velocities $V_v = \partial \Delta z_r(f_i, t) / \partial t$ changed to the opposite ones (see Figures 1a and 2b). This leads to a reduction of the plasma density depletions around the reflection and UH heights, the depletions relaxed and disappeared in $\sim 15 - 40$ s after pump wave turns off.

5 Conclusions

The results can be briefly summarized as follows. It was obtained that during all cycles the pump wave-plasma interaction developed most quickly (in a few milliseconds) after QCW switching on in the vicinity of the pump wave reflection height z_{r_0} . It is accompanied by the plasma expulsion from the interaction region (RD appearance) and by the NCp SEE feature generation. At this time there were no essential differences between cycles with different f_0 . Both the expulsion and NCp shall be attributed to the excitation of L waves due to the ponderomotive parametric instability near the PW reflection height z_{r_0} .

Later, in a 1-5 s after the QCW was switched on, for $f_0 < 4f_c$, the plasma expulsion from a vicinity of the upper hybrid height z_{UH} (UHD development) began along with development of the AA, UH-related SEE features such as DM, 2DM, UM and BC, as well as with suppression (overshoot) of the NCp feature and slowing down of expulsion from the vicinity of z_{r_0} . At 3-10 s the UHDs became deeper than the RDs. The expulsion from upper hybrid height continues until the end of 45-s-long QCW-pumping. All these effects are related to excitation of the striations and UH plasma waves. The slowing down of the z_{r_0} uplifting, RD deepening and NCp suppression indicated that the UH-related processes led to the noticeable shielding of the reflection point from the pump wave energy. A sequence of the described effects is consistent with a general scenario of the phenomena developing in the HF-pumped ionosphere (Frolov et al., 1997; Thidé et al., 2005; Grach et al., 2016) and is clearly illustrated by Sergeev et al. (2016), where the results of 3 successive 2-minute cycles at the frequency $f_0 = 5500$ kHz obtained on the same experiment (2014/06/04, 15:40-15:46 AKDT) were presented. Similar results were obtained also at the SURA facility (A. Shindin et al., 2012). In the described experiment during the cycles at $f_0 < 4f_c$ the RD and NCp develop similarly to the cycles at $f_0 = 5500$ kHz till $t = 5-10$ s, but later the RD started to deepen again, concurrently with UHD deepening on the background of plasma density decrease in the interval $z_{UH} \lesssim z \lesssim z_{r_0}$. A dependence $\delta N(z)$ looked as two isolated minima, close, respectively, to the reflection and UH heights. Note that for presented cycles at $f_0 < 4f_c$ (with approximately same initial UH heights ~ 225 km) the expulsion parameters $\Delta z(f_i)$ and $\Delta N(z)$ as well the AA behaved similarly, even quantitatively, while the SEE spectra are different. This points on a weak dependence on the AIT peculiarities on in the range $-150 \lesssim \Delta f_c \lesssim -60$ kHz.

In the single cycle with $f_0 > 4f_c$ ($f_0 = 5730$ kHz, $\Delta f_c \sim 75$ kHz) the $\delta N(z)$ developed, again, as two isolated minima, RD and UHD. In this cycle the UHD depth remained less than the RD depth during the whole OCW pumping interval; the altitude ranges, occupied by depletions, were wider, the AA of the diagnostic pulses (DW) was stronger (by ~ 10 dB) and occupied larger frequency range than at $f_0 < 4f_c$. The uplifting of the diagnostic waves (DW) reflection heights z_{ri} near the PW UH height started after ~ 15 s delay (Fig. 3c, row 4) after QCW switch on. This points to the essential difference in the AIT excitation for $f_0 > 4f_c$ and $f_0 < 4f_c$.

For the cycle at $f_0 = 5660$ kHz the PW frequency was close to $4f_c$, i.e. got into the “resonance range”, where the DM was totally suppressed or very weak, but the BUM and UM were present in the SEE spectra. Taking $f_{DM} = f_0 - \Delta f_{DM} \approx 4f_c(z_{UH}) \approx 5650$ kHz and using IGRF model we obtain $z_{UH} \approx 239$ km in the beginning of the cycle. In this cycle the DW frequency range with negative f_{di} expanded from the PW frequency f_0 (Fig. 1a, 3rd row), the temporal behavior of $\delta N(z, t)$ demonstrated deepening quasi-periodic structure with a period $\sim 3\text{--}4$ km, with amplitude growing in time and decreasing downward from z_{r0} , and occupying height interval exceeding spacing between z_{r0} and z_{UH} . Unfortunately, the total range of the diagnostic signals available for the phase data processing was too narrow to estimate lower boundary of the height interval. “Independent” z_{ri} uplifting for $z_{ri} \sim z_{UH}$ wasn’t resolved for this cycle. Therefore, for $f_0 \approx 4f_c$, the plasma expulsion from the UH region is quenched as well as the DM generation. The AA, and hence the striations developed slower, than at f_0 far from gyroharmonic, but attained quite large values till the end of QCW pumping, the AA value G achieved ~ 20 dB in DW frequency range $-150 \text{ kHz} < f_i - f_0 < 50 \text{ kHz}$.

Assuming that the height of greatest plasma expulsion corresponds to maximum PW energy consumption by ionospheric plasma we can conclude that for $f_0 < 4f_c$ the most effective PW energy input occurs initially near the PW reflection height z_{r0} . Then the energy input becomes more effective near the UH height z_{UH} . Later, when the plasma expulsion develops in the whole interval $z_{UH} \lesssim z \lesssim z_{r0}$, some kind of mutual influence of these two separated regions is, presumably, observed. For $f_0 > 4f_c$ these two isolated regions remained independent, although the UHD occupied greater altitude range. For $f_0 \approx 4f_c$ the PW energy contributed mainly near z_{r0} . The AIT excitation near the UH height is suppressed.

Finally, combined investigations of the HF heated volume by MDS, SEE and AA allow establishing interconnection between different manifestations of the AIT, and determining position (altitude) of the most effective pump wave energy input in the HF-pumped ionosphere as dependent on the offset between f_0 and nf_c .

The reasons for observed plasma expulsion is the enhancement of the gas-kinetic pressure due to electron heating and of the averaged high-frequency (ponderomotive) pressure, the enhancement is conditioned by the excitation of plasma (L and UH) waves by the pump wave near its reflection and UH heights (Dimant Ya., 1989; Grach et al., 1989; Vas’kov & Dimant, 1989). However, for adequate description of the dynamics of the electron density profile modification near PW resonances, further theoretical efforts are required.

Acknowledgments

AS, ES, SG were supported by Russian Science Foundation grant No 20-12-00197 (sections 1,4,5), by Russian Foundation for Basic Research grants No 19-02-00343 (section 2) and No 20-32-70198 (section 3). PB, CS and MM were supported by the NRL 6.1 Basic Research Program (experimental work). Source data and code for reproducing the figures can be found in A. V. Shindin (2021).

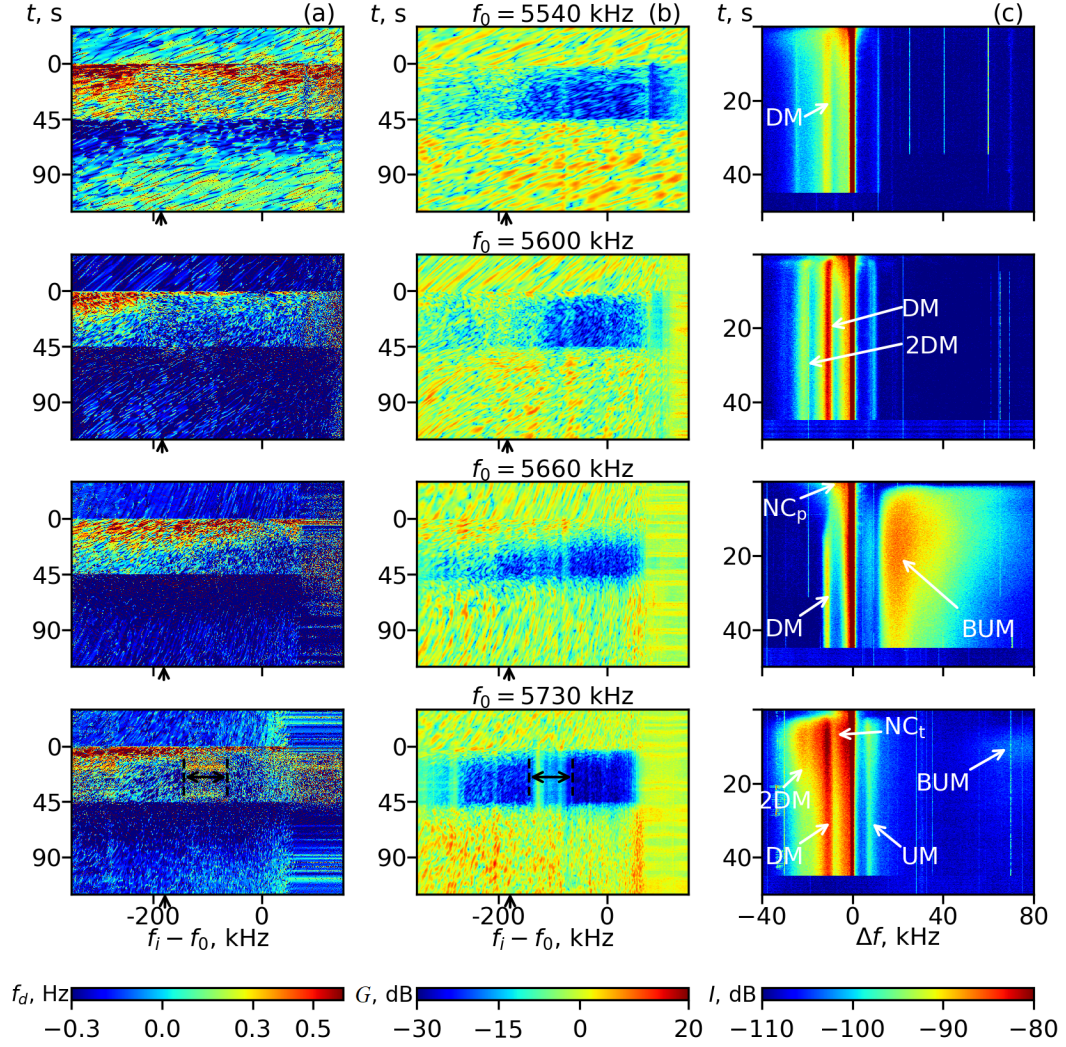


Figure 1. Column (a): the Doppler frequency shifts (colors) vs. time t and diagnostic wave spectral component frequency shift $f_i - f_0$. Column (b): normalized amplitude of diagnostic waves G (color) vs. t and frequency shift $f_i - f_0$. Column (c): the SEE spectrograms. The PW frequencies f_0 are shown above b-panels. Double arrows show contaminated frequency range for phase data processing.

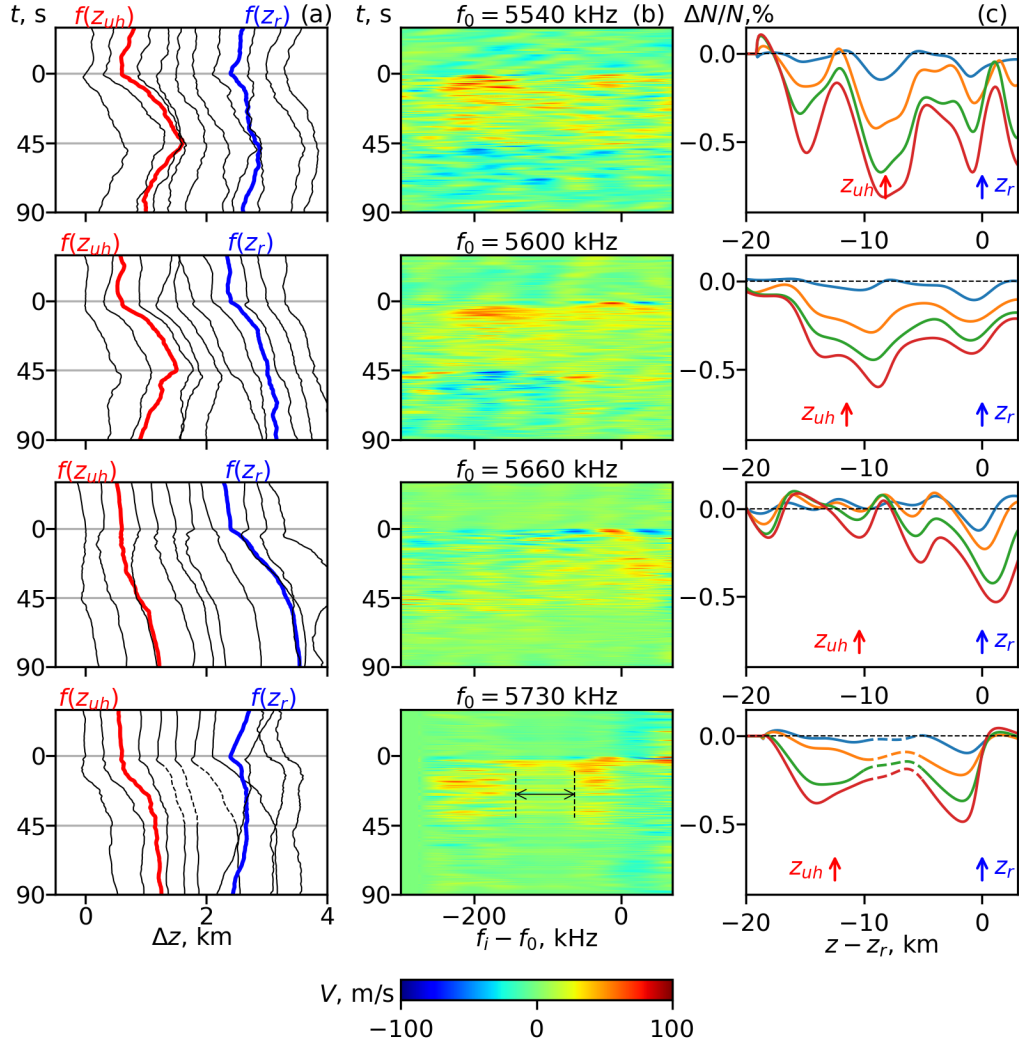


Figure 2. Column (a): temporal variations of the reflection heights of different spectral components of sounding pulses $\Delta z(f_i, t)$ for different cycles. Frequency step between shown spectral components $\Delta f_i = 60$ kHz starting from f_0 . Additional height shift 300 m between reflection heights of the successive shown frequencies f_i at $t = 0$ is added for clarity. Red and blue lines correspond the spectral components reflected from z_{UH} and z_r . Column (b): velocity of the sounding waves reflection height displacement $V_v = \partial \Delta z_r(f_i, t) / \partial t$ vs. time and frequency. Column (c): relative variations of electron density $[N(t) - N(0)] / N(0)$ vs. height at $t = 5$ s (blue), 15 s (orange) 30 s (green) and 45 s (red) in the same cycles. Double arrow and dashed parts of lines show contaminated frequency range.

References

- Berezin, I. V., Beliansky, V. B., Budko, N. I., & Vaskov, V. V. (1991). Diagnostics of the process of excitation of plasma-oscillations by the field of a powerful radio wave. *Geomagnetism and Aeronomy*, 31(5), 874-880.
- Carozzi, T. D. (2002). Stimulated electromagnetic emissions during pump frequency sweep through fourth electron cyclotron harmonic. *Journal of Geophysical Research*, 107(A9). doi: 10.1029/2001ja005082
- Dimant Ya., S. (1989). Vzaimodeistvie vysokochastotnykh radiovoln s ionosferoi (interaction of high-frequency radiowaves with the ionosphere). In E. E. Tsedilina (Ed.), (p. 19-39). IZMIRAN.
- Frolov, V. L. (2004). Ponderomotive narrow continuum (NCp) component in stimulated electromagnetic emission spectra. *Journal of Geophysical Research*, 109(A7). doi: 10.1029/2001ja005063
- Frolov, V. L., Bakhmet'eva, N. V., Belikov, V. V., Vertogradov, G. G., Vertogradov, V. G., Komrakov, G. P., ... Khudukon, B. Z. (2007). *Physics-Uspekhi*, 50(3), 315. doi: 10.1070/pu2007v050n03abeh006282
- Frolov, V. L., Erukhimov, L. M., Metev, S. A., & Sergeev, E. N. (1997, dec). Temporal behaviour of artificial small-scale ionospheric irregularities: Review of experimental results. *Journal of Atmospheric and Solar-Terrestrial Physics*, 59(18), 2317-2333. doi: 10.1016/s1364-6826(96)00126-5
- Frolov, V. L., Sergeev, E. N., Ermakova, E. N., Komrakov, G. P., & Stubbe, P. (2001, aug). Spectral features of stimulated electromagnetic emission, measured in the 4.3-9.5 MHz pump wave frequency range. *Geophysical Research Letters*, 28(16), 3103-3106. doi: 10.1029/2001gl013251
- Ginzburg, V. L. (1970). *The propagation of electromagnetic waves in plasmas*. Oxford, New York: Pergamon Press.
- Grach, S. M., Komrakov, G. P., Yurishchev, M. A., Thidé, B., Leyser, T. B., & Carozzi, T. (1997, feb). Multifrequency doppler radar observations of electron gyroharmonic effects during electromagnetic pumping of the ionosphere. *Physical Review Letters*, 78(5), 883-886. doi: 10.1103/physrevlett.78.883
- Grach, S. M., Mityakov, N. A., Rapoport, V. O., & Trakhtengert, V. Y. (1981, jan). Thermal parametric turbulence in a plasma. *Physica D: Nonlinear Phenomena*, 2(1), 102-106. doi: 10.1016/0167-2789(81)90063-4
- Grach, S. M., Mityakov, N. A., & Shvarts, M. M. (1989). Plasma density jump at the stage of developed of thermal parametric instability (in russian). *Geomagnetism and Aeronomy*, 29, 453-457.
- Grach, S. M., Sergeev, E. N., Mishin, E. V., & Shindin, A. V. (2016, nov). Dynamic properties of ionospheric plasma turbulence driven by high-power high-frequency radiowaves. *Physics-Uspekhi*, 59(11), 1091-1128. doi: 10.3367/ufne.2016.07.037868
- Grach, S. M., Sergeev, E. N., Yashnov, V. A., & Kotov, P. V. (2008, jul). Spectra of stimulated electromagnetic emission of the ionosphere sweeping of the pump wave frequency near gyroharmonics. II. discussion of the results. *Radiophysics and Quantum Electronics*, 51(7), 499-514. doi: 10.1007/s11141-008-9058-y
- Gurevich, A. V. (2007, nov). Nonlinear effects in the ionosphere. *Physics-Uspekhi*, 50(11), 1091-1121. doi: 10.1070/pu2007v050n11abeh006212
- Korn, G. A., & Korn, T. M. (2000). *Mathematical handbook for scientists and engineers: Definitions, theorems, and formulas for reference and review*. DOVER PUBN INC. Retrieved from https://www.ebook.de/de/product/3344668/granino_a_korn_theresa_m_korn_mathematical_handbook_for_scientists_and_engineers_definitions_theorems_and_formulas_for_reference_and_review.html
- Kotov, P. V., Sergeev, E. N., & Grach, S. M. (2008, jun). Spectra of stimulated electromagnetic emission of the ionosphere upon sweeping of the pump wave

- frequency near gyroharmonics. i. experimental results. *Radiophysics and Quantum Electronics*, 51(6), 417–430. doi: 10.1007/s11141-008-9043-5
- Leyser, T. B. (2001). *Space Science Reviews*, 98(3/4), 223–328. doi: 10.1023/a:1013875603938
- Leyser, T. B., Thidé, B., Derblom, H., Hedberg, Å., Lundborg, B., Stubbe, P., ... Rietveld, M. T. (1989, sep). Stimulated electromagnetic emission near electron cyclotron harmonics in the ionosphere. *Physical Review Letters*, 63(11), 1145–1147. doi: 10.1103/physrevlett.63.1145
- Leyser, T. B., Thidé, B., Waldenvik, M., Goodman, S., Frolov, V. L., Grach, S. M., ... Kotik, D. S. (1993). Spectral structure of stimulated electromagnetic emissions between electron cyclotron harmonics. *Journal of Geophysical Research*, 98(A10), 17597. doi: 10.1029/93ja01387
- Leyser, T. B., Thidé, B., Waldenvik, M., Veszelei, E., Frolov, V. L., Grach, S. M., & Komrakov, G. P. (1994). Downshifted maximum features in stimulated electromagnetic emission spectra. *Journal of Geophysical Research*, 99(A10), 19555. doi: 10.1029/94ja01399
- Lobachevsky, L. A., Gruzdev, Y. V., Kim, V. Y., Mikhaylova, G. A., Panchenko, V. A., Polimatidi, V. P., ... Kopka, H. (1992, jan). Observations of ionospheric modification by the tromsø heating facility with the mobile diagnostic equipment of IZMIRAN. *Journal of Atmospheric and Terrestrial Physics*, 54(1), 75–85. doi: 10.1016/0021-9169(92)90086-z
- Sergeev, E. N., Frolov, V. L., Grach, S. M., & Kotov, P. V. (2006, jan). On the morphology of stimulated electromagnetic emission spectra in a wide pump wave frequency range. *Advances in Space Research*, 38(11), 2518–2526. doi: 10.1016/j.asr.2005.02.046
- Sergeev, E. N., Grach, S. M., Kotov, P. V., Komrakov, G. P., Boiko, G. N., & Tokarev, Y. V. (2007, aug). Diagnostics of the HF-pumped ionospheric region using wide-band radio emission. *Radiophysics and Quantum Electronics*, 50(8), 593–610. doi: 10.1007/s11141-007-0052-6
- Sergeev, E. N., Shindin, A. V., Grach, S. M., Milikh, G. M., Mishin, E. V., Bernhardt, P. A., ... McCarrick, M. J. (2016, jul). Exploring HF-induced ionospheric turbulence by doppler sounding and stimulated electromagnetic emissions at the high frequency active auroral research program heating facility. *Radio Science*, 51(7), 1118–1130. doi: 10.1002/2015rs005936
- Shindin, A., Sergeev, E., & Grach, S. (2012, aug). Applications of broadband radio signals for diagnostics of electron density profile dynamics and plasma motion in the HF-pumped ionosphere. *Radio Science*, 47(6), n/a–n/a. doi: 10.1029/2011rs004895
- Shindin, A. V. (2021, May). *Multifrequency Doppler Sounding data & software (HAARP 06/04/14 experiments)*. Zenodo. Retrieved from <https://doi.org/10.5281/zenodo.4809544> doi: 10.5281/zenodo.4809544
- Streltsov, A. V., Berthelier, J.-J., Chernyshov, A. A., Frolov, V. L., Honary, F., Kosch, M. J., ... Rietveld, M. T. (2018, oct). Past, present and future of active radio frequency experiments in space. *Space Science Reviews*, 214(8). doi: 10.1007/s11214-018-0549-7
- Stubbe, P., Kopka, H., Thidé, B., & Derblom, H. (1984, sep). Stimulated electromagnetic emission: A new technique to study the parametric decay instability in the ionosphere. *Journal of Geophysical Research: Space Physics*, 89(A9), 7523–7536. doi: 10.1029/ja089ia09p07523
- Thidé, B., Kopka, H., & Stubbe, P. (1982, nov). Observations of stimulated scattering of a strong high-frequency radio wave in the ionosphere. *Physical Review Letters*, 49(21), 1561–1564. doi: 10.1103/physrevlett.49.1561
- Thidé, B., Sergeev, E. N., Grach, S. M., Leyser, T. B., & Carozzi, T. D. (2005, dec). Competition between langmuir and upper-hybrid turbulence in a high-frequency-pumped ionosphere. *Physical Review Letters*, 95(25), 255002. doi:

- 10.1103/physrevlett.95.255002
- 518 Tikhonov, A. N. (1995). *Numerical methods for the solution of ill-posed problems*.
519 Dordrecht: Springer Netherlands.
520
- 521 Vas'kov, V. V., & Dimant, Y. S. (1989). Effect of the deformation of the normal
522 profile of the ionosphere plasma on the anomalous absorption of a high-power
523 radiowave in the resonance region. *Geomagnetizm and Aeronomy*, 29, 373-
524 377.
- 525 Vaskov, V. V., Golian, S. F., Gurevich, A. V., Dimant, I. S., & Ziuzin, V. A. (1986,
526 June). Excitation of upper hybrid resonance in the ionospheric plasma by an
527 intense radio wave. *ZhETF Pisma Redaktsiiu*, 43, 512-515.